NASA
Technical
Paper
2169

AUGUST 1983

Time Dependence of Solid-Particle Impingement Erosion of an Aluminum Alloy

P. Veerabhadra Rao
and Donald H. Buckley

NASA

25th Anniversary
1958-1983

NASA
Technical
Paper
2169

1983

Time Dependence of Solid-Particle Impingement Erosion of an Aluminum Alloy

P. Veerabhadra Rao
and Donald H. Buckley
Lewis Research Center
Cleveland, Ohio

NASA
National Aeronautics
and Space Administration
**Scientific and Technical
Information Branch**
1983

Summary

Erosion and morphological studies of 6061-T6511 aluminum alloy eroded by normal impingement jets of spherical glass beads and angular crushed-glass particles were conducted. Erosion morphology (pit width, pit depth, and width-depth ratio) was studied at different gas pressures in order to investigate fully the effect of time on erosion rate. The eroded surfaces were studied with a scanning electron microscope, and surface profiles were measured with a profilometer. A large amount of experimental data reported in the literature was also analyzed in order to understand the effect of variables such as the type of device, the erodent particle size and shape, the impact velocity, and the abrasive charge on erosion-rate-versus-time curves.

Pit-width-versus-time or pit-depth-versus-time curve trends were similar to erosion-versus-time curve trends for glass bead impingement. Pit-depth-versus-time curve trends were similar to erosion-rate-versus-time curve trends for crushed-glass impingement. Analysis of the present experimental data resulted in three types of erosion-rate-versus-time curves: (1) curves with incubation, acceleration, and steady-state periods (type I); (2) curves with incubation, acceleration, deceleration, and steady-state periods (type III); and (3) curves with incubation, acceleration, peak rate, and deceleration periods (type IV). The type IV curve is less frequently seen and had not been reported in the literature. Analysis of extensive literature data generally indicated three types of erosion-rate-versus-time curves. Two types (types I and III) were observed in the present study; the third type involves incubation (with deposition), acceleration, and steady-state periods (type II). Analysis of data from present experiments and from the literature indicated that the incubation (with or without deposition) and acceleration periods increased with decreasing particle impact velocity. Data analyses from the present investigation and from the literature further provided the understanding that the corresponding stages or periods of erosion must be considered for meaningful correlations and characterization of the erosion resistance of ductile materials.

Introduction

Solid-particle impingement erosion of ductile materials used in the petrochemical and coal gasification industries has been studied by a number of investigators, and full reviews are given in references 1 to 4. The most important aspects considered thus far have been the effects of particle size and shape, abrasive charge, impingement angle, impact velocity, and the material properties of both the specimen and the erodent. The main purpose of testing materials has been to understand the erosion mechanism in general and to characterize the erosion resistance of materials in particular for a variety of applications (e.g., fluidized beds, nozzle flows, and pneumatic transport in pipes). The effect of exposure time or abrasive charge on the weight loss or erosion rate is essential not only to understanding precisely the different stages or periods of erosion with time for correlation and characterization purposes, but also to modeling and extrapolating laboratory data more precisely to field conditions. (Weight loss, erosion, and volume loss as well as stage and period have been used interchangeably throughout this report.) The effect of exposure time or abrasive charge on the weight loss of different materials has been studied since the 1950's (refs. 5 to 8). (Exposure time and abrasive charge have been used interchangeably.) The basic definitions of erosion periods are not universal. Recently references 1 and 2, however, precisely defined the periods contributing to a better understanding of the erosion rate stages.

Typical plots of cumulative weight or volume loss versus time or abrasive charge generally found in the literature are schematically shown in figure 1. Schematics of volume loss rate versus exposure time for the curves in figure 1 are shown in figure 2. In general, the course of a solid-particle impingement erosion process on ductile metals can be characterized by the following periods:

(1) Incubation or induction period—the exposure time span or abrasive charge during which there is a little or no weight loss. In fact, in a few cases there can be a slight weight gain caused by deposition or embedment of particles.

(2) Acceleration or accumulation period—the exposure time span in which the weight loss rate increases rapidly.

(3) Deceleration or attenuation period—the exposure time span in which the weight loss rate decreases rapidly.

(4) Steady-state period—the long time span in which the weight loss rate becomes constant and continuous (sometimes at a lower rate than peak, fig. 2(c)). This is the period commonly referred to as the "maximum rate" or "constant rate" period.

In this report, the curves in figures 2(a), (b), and (c) are referred to as types I, II, and III, respectively. Type I consists of incubation, acceleration, and steady-state periods; type II of incubation (with deposition), acceleration, and steady-state periods; and type III of incubation, acceleration, deceleration, and steady-state periods.

In most previous tests of solid-particle impingement erosion the test has been continued until the maximum rate of erosion has been established (ref. 2). This has been accomplished by running the test for successive equal time steps and obtaining the same value of weight loss for these steps. However, a systematic study to compare the effects of time on erosion rate for different materials with

various types of particles and experimental devices had not previously been undertaken.

The different types of weight-loss-rate-versus-time curves deduced from the weight-loss-versus-time curves reported in the literature and a limited discussion of overall erosion-versus-time curves has never fully clarified the various types of curves. Furthermore lack of universal definitions of the different stages has caused misunderstanding. This lack of complete understanding motivated the study reported herein.

The present investigation reports erosion-rate-versus-time curves for a 6061-T6511 aluminum alloy undergoing glass-bead and crushed-glass jet impingement at normal incidence. This alloy has been well characterized and is similar in microstructure and strength at room temperature to the 300 series stainless steels used in coal gasification internal components at temperatures to 1000° C. The study of pit morphology (pit width, pit depth, and width-depth ratio) and use of scanning electron microscopy (SEM) provided a good insight into the erosion-rate-versus-time curves. Extensive normal-incidence erosion data from the literature on a wide spectrum of ductile materials tested at different experimental conditions were analyzed to arrive at a better understanding of the erosion-rate-versus-time curves and to confirm the present experimental results with the aluminum alloy. This report also discusses whether it is necessary to consider the corresponding stages of the erosion-rate-versus-time curves in order to correlate erosion data with material properties and in order to achieve a meaningful characterization of the erosion resistance of materials.

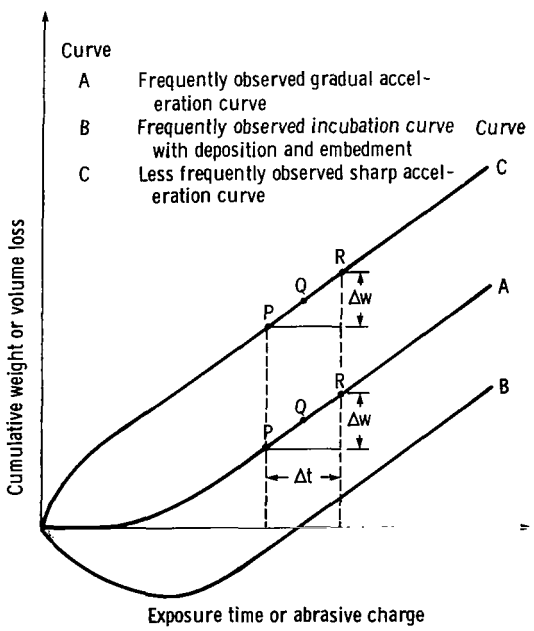

Figure 1. - Characteristic cumulative-volume-loss-versus-time curves. Instantaneous erosion rate at Q equals slope of local tangent at Q = Δw/Δt.

Literature Survey of Time Effects

Cumulative weight loss as a function of time or abrasive charge has been discussed in the literature quite often by several researchers. The experiments were conducted with different experimental devices, materials,

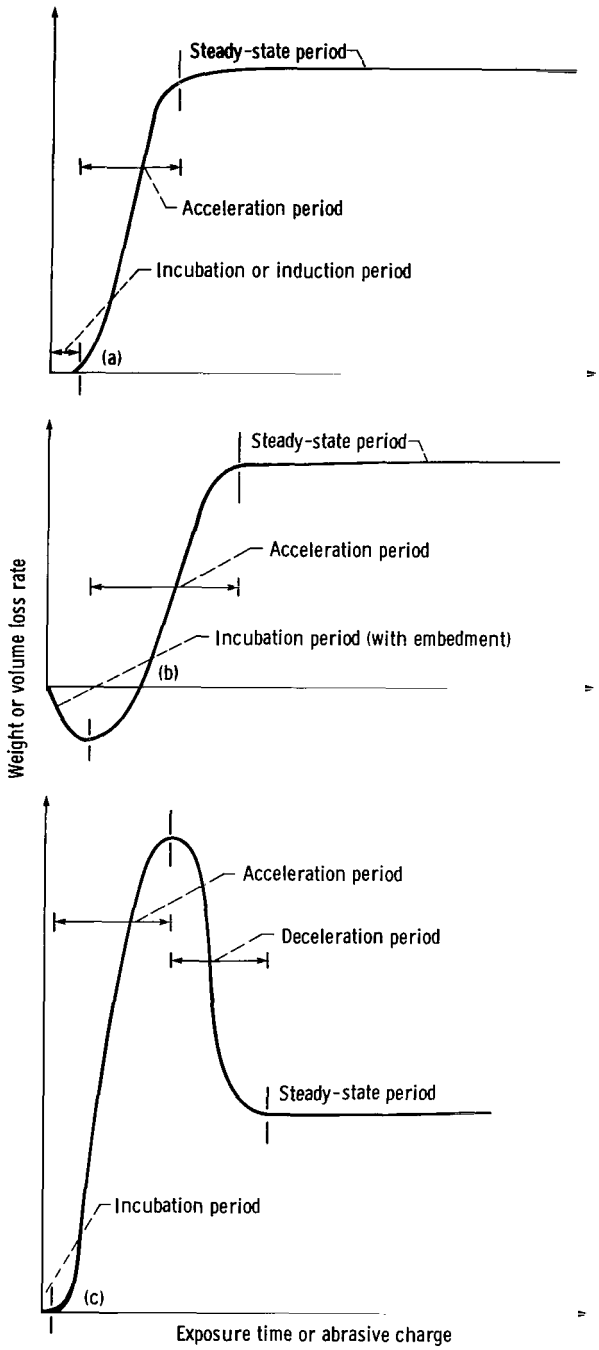

(a) Type I.
(b) Type II.
(c) Type III.

Figure 2. - Characteristic typical volume-loss-rate-versus-time curves.

erodent particle shapes, particle sizes, velocities, and impingement angles. Normal impingement studies are briefly outlined herein.

Finnie (refs. 5 and 6) presents weight-loss-versus abrasive charge plots for SAE 1020 and AISI 1045 steels impacted by 250-μm angular SiC particles. Neilson and Gilchrist (ref. 9) tested aluminum; Ives and Ruff (ref. 10) and Carter et al. (ref. 11), copper; and Kosel et al. (ref. 12), nickel with angular Al_2O_3 particles. Carter et al. plotted weight-loss-versus-exposure-time curves; and the others (refs. 9, 10, and 12), weight-loss-versus-abrasive-charge curves. Tilly (ref. 13) and Tilly and Sage (ref. 14) eroded chromium steel, aluminum, cobalt alloy, and several plastics with 60- to 125-μm angular quartz particles and report weight-loss-versus-abrasive-charge curves. Rickerby and Macmillan (ref. 15) tested pure aluminum, and Hutchings (ref. 16) eroded aluminum alloy with 1.58-mm WC spheres and 495- to 600-μm spherical glass beads, respectively. Reference 15 presents weight-loss-versus-number-of-impact curves, and reference 16 presents mass-loss-versus-glass-bead-particle-charge curves. Brown, et al. (ref. 17), investigated single-crystal copper and iron and Follansbee et al. (ref. 18), copper with 70- and 50-μm glass spheres, respectively.

Although these references discuss overall weight loss as a function of abrasive charge, only Young and Ruff (ref. 19) plotted relative-weight-loss-rate-versus-abrasive-charge curves.

Weight-loss-versus-abrasive-charge curves presented by Finnie (refs. 5 and 6) show that at 90° a certain amount of erosion must take place before the increase in weight loss is proportional to the increase in abrasive charge (i.e., to attain a steady-state period). Using SiC particles, he observed that the effect of work hardening is small as compared with surface roughening.

Duffin (ref. 7) reports weight gain (deposition) due to embedment of particles in the metal surface. With stationary targets, steady state was reached after 4 g of feldspar had impacted the metal at different temperatures and two velocities.

Others (e.g., refs. 9, 10, 13, and 14) also report initial deposition followed by a linear relation of weight loss with abrasive charge. Significantly lower abrasive flow rates would probably require the use of a longer erosion test time in order to achieve steady-state conditions (ref. 19). This may be true with low particle velocities as well. Materials commonly exhibited an increase in deposition (incubation period) with increasing impingement angle and decreasing impact velocity (refs. 9, 10, and 20). Deposition took place until the surface became saturated with abrasive particles and degraded (ref. 3).

On the other hand, some studies (refs. 8, 11, 15, 17, and 21) do not report any weight gain (deposition) with initial impact. (Finnie et al. (ref. 8) used angular particles and all other investigators used spherical particles.)

Generally, a significant incubation period has been observed for soft and ductile materials, such as annealed light alloys and plastics, in which the erosion rate is affected by the nonlinearity of erosion with time (refs. 3 and 13). The common engineering materials, including steels, do not have a discernible incubation period, and the erosion process stabilizes immediately to the steady state (ref. 3). Hence according to reference 3 it may be surmised that the erosion rate is not much affected by nonlinearity of erosion-versus-time characteristics for these particular materials.

A typical erosion-rate-versus-time curve (as in fig. 2(a)) has been reported only by Young and Ruff (ref. 19); it is discussed in reference 1 as well as by Follansbee et al. (ref. 18). Though this type of curve is less frequent, it is interesting for its practical significance. Most of the other investigators discuss erosion-rate-versus-time curves of the type shown in figure 2(a), which contain incubation, acceleration, and steady-state periods.

The detrimental effects of erosion on the material surfaces of various components used in the petrochemical and coal gasification industries are mainly governed by the type of function, the performance, and the efficiency necessary for a particular component. In some systems or components even the smallest amount of erosion or embedment may not be tolerated (e.g., optically guided systems and radomes). Others function with loss of efficiency until they break down completely (e.g., components of coal gasification systems).

Apparatus and Experimental Procedure

Specimens

Specimens of the aluminum alloy 6061-T6511 were used in the experimental part of this investigation. The aluminum alloy specimens were 6 mm thick, 25 mm wide, and 37.5 mm long. The nominal composition and mechanical properties of the aluminum alloy are given in reference 22. Before erosion exposure, all specimens were polished with 600-grit emery paper and then with 3-μm diamond paste, were cleaned with distilled water, and were air dried.

Apparatus and Procedure

A sandblasting facility was used to continuously impact test specimens with erodent particles at normal incidence. A schematic of the sandblasting nozzle arrangement is shown in figure 3. Commercial-grade no. 9 spherical glass beads of approximately 20-μm average diameter and commerical-grade no. 10 crushed glass of 30-μm average size were used. The particle size distribution of glass beads is discussed in reference 23. The SEM micrographic details of the sizes and shapes of both forms of glass are available in references 21 and 24.

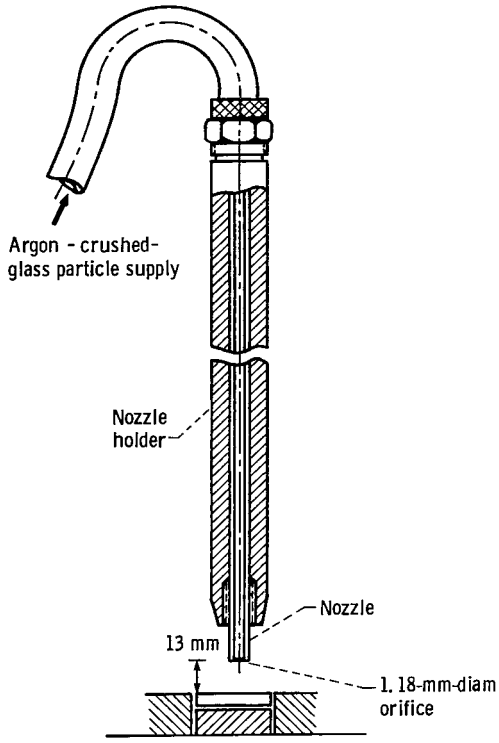

Figure 3. - Schematic diagram of nozzle holder arrangement for steady-jet impingement.

In the sandblasting facility the distance between the test specimen and the nozzle (diameter, 1.18 mm) was 13 mm. Argon was used as the driving gas from 0.14 to 0.82 MPa (gage) pressure. The velocities are obtained by using a double disk arrangement similar to one discussed in reference 25. The jet divergence was about ±2° relative to the centerline. The nozzle was replaced frequently during the experiments to limit the effect of nozzle wear on jet divergence, impact velocity, erodent flow rate, etc. The nonsymmetric erosion pit is an indirect and approximate indication of nozzle wear in this type of study.

Volume loss values were obtained by weighing specimens before and after their exposure to the erodents and dividing by density. The sensitivity of the balance was ±0.1 mg. Profiles of the eroded surfaces were recorded with a profilometer. The depths of the shallow pits were measured from surface traces and checked with a depth gage. The deep pits were always measured with a depth gage. The sensitivity of the gage was ±2.5 μm (0.0001 in.). The eroded surfaces were observed with a scanning electron microscope.

Experimental Results and Discussion

Statistical Variation of the Experimental Data

The reproducibility of the experimental data and their statistical variations are presented in references 21 and 26 for 6061-T6511 aluminum alloy examined at different driving gas pressures during glass-bead and crushed-glass particle impingement. Extensive analysis indicates that the maximum standard deviations of the volume loss data scatter are 1.4 for glass-bead impingement and 2.07 for crushed-glass particle impingement. Four specimens were examined in the former series of experiments, and a maximum of five specimens were examined in the latter experimental series. The standard deviation of the data for thermoplastic materials is presented in reference 23, wherein a maximum of eight specimens were examined in order to study data scatter. Table I presents the

TABLE I. - EXPERIMENTAL DATA SCATTER FOR 6061-T6511 ALUMINUM ALLOY CIRCULAR SPECIMENS EXAMINED AT 0.82-MPa DRIVING GAS PRESSURE (PARTICLE VELOCITY, 130 m/sec)[a]

Exposure time, min	Glass-bead flow, kg	Volume loss, m^3				Arithmetic average volume loss, m^3	Standard deviation of volume loss	Variance of volume loss
		Specimen						
		1	2	3	4			
5	0.143	2.73×10^{-9}	3.03×10^{-9}	3.32×10^{-9}	3.95×10^{-9}	3.26×10^{-9}	0.52	0.203
10	.285	8.16	7.90	7.53	8.08	7.92	.28	.059
15	.427	12.80	12.80	13.39	14.28	13.32	.70	.367
20	.570	19.30	19.30	19.19	19.19	19.25	.06	.003
25	.712	24.65	24.24	25.35	25.17	24.85	.51	.191
30	.855	29.89	30.41	31.33	30.18	30.45	.62	.291
35	.997	35.06	35.20	37.49	35.94	35.92	1.11	.931
40	1.140	42.03	40.48	42.40	41.25	41.54	.85	.547
45	1.282	46.68	44.98	47.08	46.61	46.34	.92	.646
50	1.425	51.88	50.18	51.51	51.70	51.32	.77	.448
55	1.567	57.05	55.06	56.35	56.46	56.23	.84	.527
60	1.709	65.57	61.99	63.58	63.25	63.60	----	-----

[a]Specimens 25.4 mm in diameter and 37.5 mm long were studied. The variance was calculated by using the equations:

$$\text{Variance} = \Sigma x^2/N - (\Sigma x)^2/N^2$$

$$\text{Standard deviation} = \sqrt{\text{Variance} \times N/(N-1)}$$

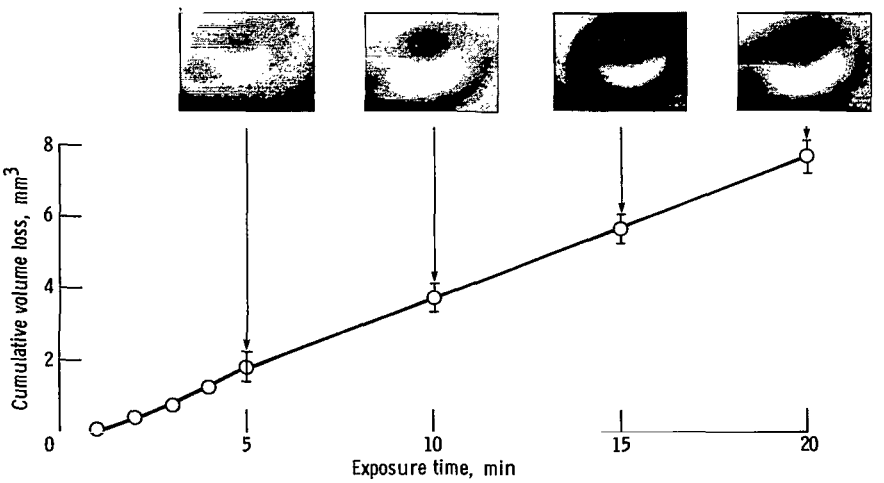

Figure 4. - Cumulative volume loss as a function of exposure time.

arithmetic average, the standard deviation, and the variance with respect to time of four 6061-T6511 aluminum alloy cylinders exposed to glass-bead impingement. The maximum standard deviation of volume loss was 1.11 over the entire test duration. The individual volume loss variations of each specimen clearly indicate the good reproducibility of the experimental data during solid-particle impingement. It is further observed from table I that the experimental data scatter does not abruptly change the course of any trend and does not result in data fluctuations.

Erosion-Rate-Versus-Time Curves

Spherical particle impingement. – A typical cumulative-volume-loss-versus-exposure-time curve of an aluminum alloy specimen exposed to glass-bead jet impingement at 0.27-MPa pressure (particle velocity = 72 m/sec) is presented in figure 4 (ref. 21). The micrographs depicting the morphological features of the erosion pits are also presented in this figure. The width, depth, and width-depth ratio of the pit at this pressure condition are given in table II.

The instantaneous-volume-loss-rate-versus-exposure-time curve is presented in figure 5. The instantaneous volume loss was calculated as the slope of the local tangent (fig. 1). Figure 5 is similar to figure 2(c): it is a type III curve consisting of four zones—incubation, acceleration, deceleration, and steady state. As mentioned earlier, this type of curve has been discussed in the literature (refs. 1, 18, and 19) on stainless steel and copper.

TABLE II. - EROSION PIT WIDTHS, DEPTHS, AND THEIR RATIOS

[Aluminum alloy specimen impinged with a jet of glass beads at 0.27 MPa for different time intervals.]

Exposure time, min	Width of pit[a], W, μm	Depth of pit[a], d, μm	W/d
1	3564	53	68.9
2	4135	124	33.3
3	4224	201	21.0
4	4331	216	20.1
5	4445	264	16.8
10	5186	470	11.0
15	5463	635	8.6
20	5926	810	7.3

[a]Pit widths and depths were converted to micrometers from inches.

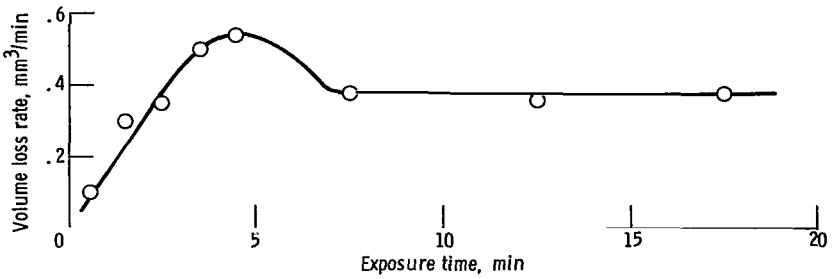

Figure 5. - Instantaneous volume loss rate as a function of exposure time.

Width, depth, and width-depth ratio as a function of exposure time are shown in figure 6, and the growth rates of the same parameters with time are shown in figure 7. Comparing figure 4 with figure 6 and figure 5 with figure 7 provides a good insight into the erosion process with time. The initial spike of the volume loss rate is probably due to the rapidly increasing width, depth, and width-depth ratio of the pit with time. The glass-bead flow rate

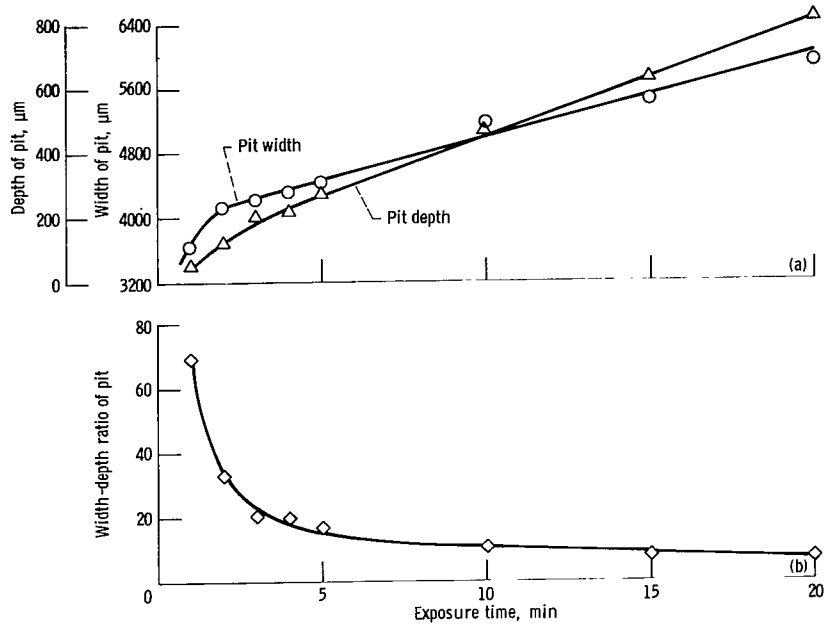

(a) Pit width or pit depth.
(b) Pit width-depth ratio.

Figure 6. - Pit width, pit depth, and their ratio as a function of exposure time.

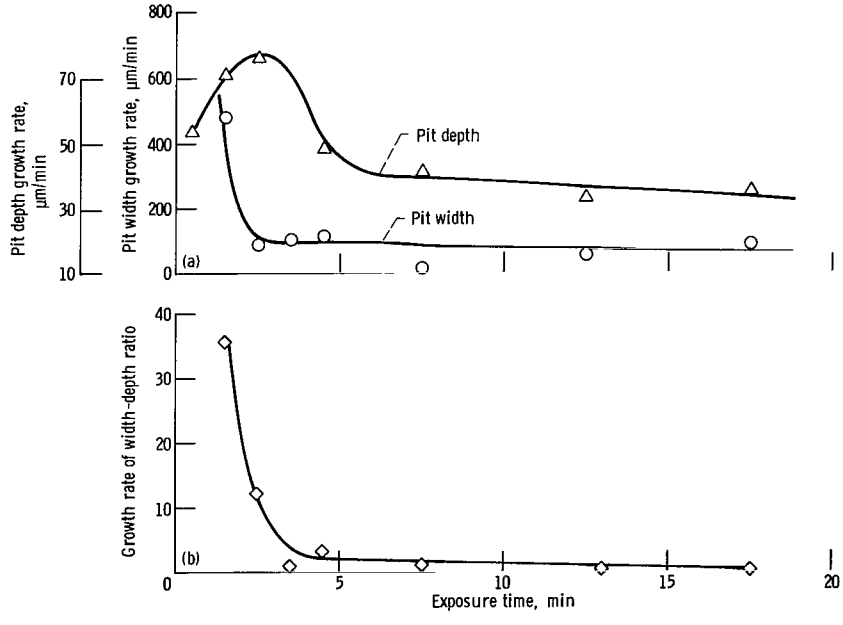

(a) Pit width or pit depth.
(b) Pit width-depth ratio.

Figure 7. - Instantaneous growth rates of pit width, pit depth, and their ratio as a function of exposure time.

was highest at the 0.27-MPa pressure condition. This may also be responsible for the initial spike.

It is easy to suspect the influence of periodic impingement and the statistical variation of the experimental data on the observed initial spike. However, a systematic study to determine the effect of periodic impingement on the volume-loss-rate-versus-exposure-time curves of metals and plastics revealed similarity in erosion characteristics to those generally occurring in airblasting (ref. 14). As discussed earlier, the standard deviation of the experimental data was less pronounced than the trend of the curve. Hence, it can be assumed that the volume-loss-rate-versus-exposure-time curve observed is a characteristic of pit morphology and related influences rather than a result of periodic impingement and experimental data scatter.

The cumulative-erosion-versus-time curve (fig. 4) is similar to the pit-width-versus-time and pit-depth-versus-time curves (fig. 6(a)), including the linear portions of the curves. Hence it is possible to assume that these curves approximately represent erosion-versus-time curves but to a different scale during solid particle jet impingement. Under different experimental conditions (ref. 19) measurements of specimen weight loss and pit depth as a function of abrasive flow have shown a complicated relationship. It is evident from figure 7(b) that as the width-depth ratio of the pit ceases to increase with time, the erosion rate attains a steady state.

Instantaneous volume-loss-rate-versus-time curves of an aluminum alloy at different pressures during glass-bead jet impingement are shown in figure 8. The curves in this figure exhibit acceleration and steady-state periods similar to those of type I curves (fig. 2(a)). Most analyses of erosion data on aluminum and aluminum alloy impacted with spherical particles (refs. 15 and 16) result in curves identical to these. Other studies, using both spherical (ref. 17) and angular (refs. 3, 5 to 9, and 13) particles, also produced similar weight-loss-versus-abrasive-charge curves.

Instantaneous pit depth rate, pit width rate, and the width-depth ratio are plotted with respect to time in figures 9 to 11. Because the rates of pit depth and width did not change much, the erosion rates tended to stabilize. As the pressure of the jet increased, the width-depth ratio of a pit reached a limiting value. From the morphological studies (ref. 21) it is evident that the appearance of "radially concentric rings" inside the pit and platelet removal approximately coincide with the "steady state" erosion rate period.

Rickerby and Macmillan (ref. 15) state that after erosion begins, an ever-decreasing amount of additional strain hardening takes place as subsequent impacts harden and reduce the extent of those areas not yet fully hardened. This condition gradually increases the extent of platelet formation and causes the erosion to attain its steady-state value.

Crushed-glass impingement. – Aluminum specimens were impacted with a jet of angular crushed-glass particles at 0.14, 0.27, 0.41, 0.54, 0.68, and 0.82 MPa (ref. 26). The resulting instantaneous-volume-loss-rate-versus-time curves are presented in figure 12. These curves are different from the curves in figure 2 and were neither discussed nor reported by earlier investigators. Analyses of data on various materials eroded by different

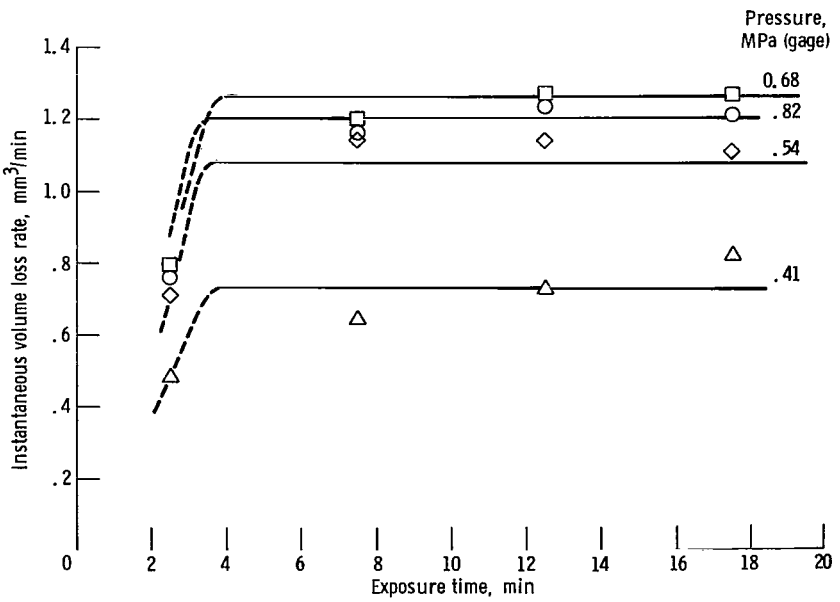

Figure 8. - Instantaneous volume loss rate as a function of exposure time for aluminum alloy exposed to jet of glass beads at different pressures.

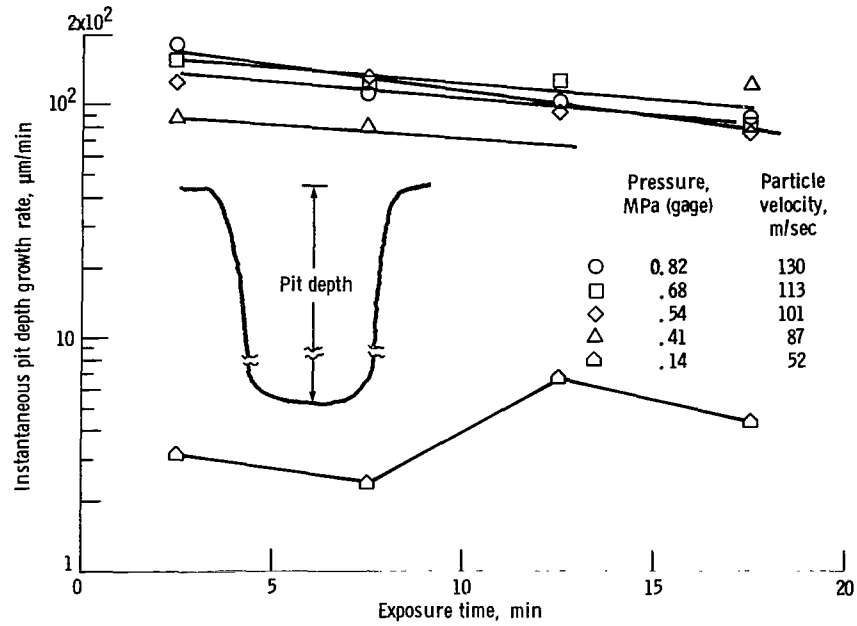

Figure 9. - Instantaneous pit depth growth rate as a function of exposure time for aluminum alloy exposed to jet of glass beads at different pressures.

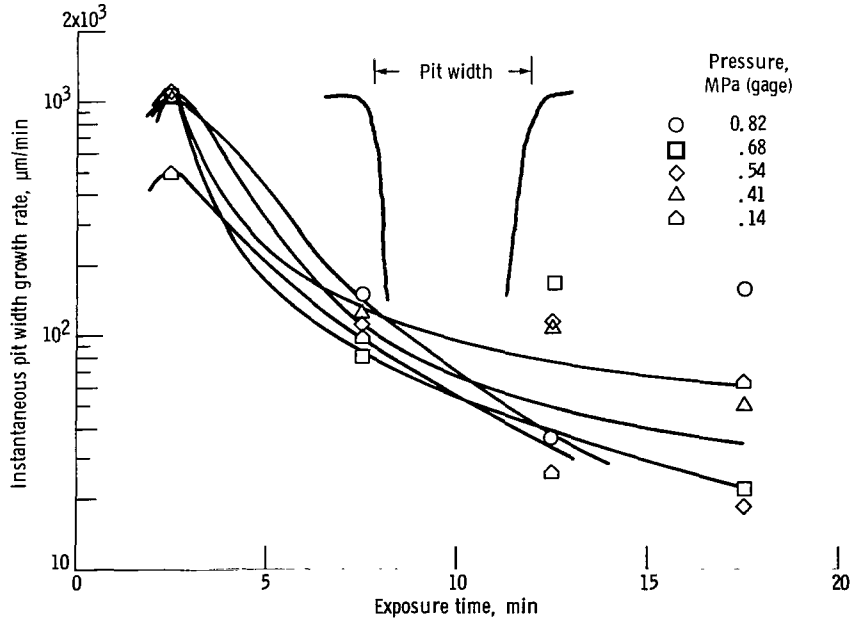

Figure 10. - Instantaneous pit width growth rate as a function of exposure time for aluminum alloy exposed to jet of glass beads at different pressures.

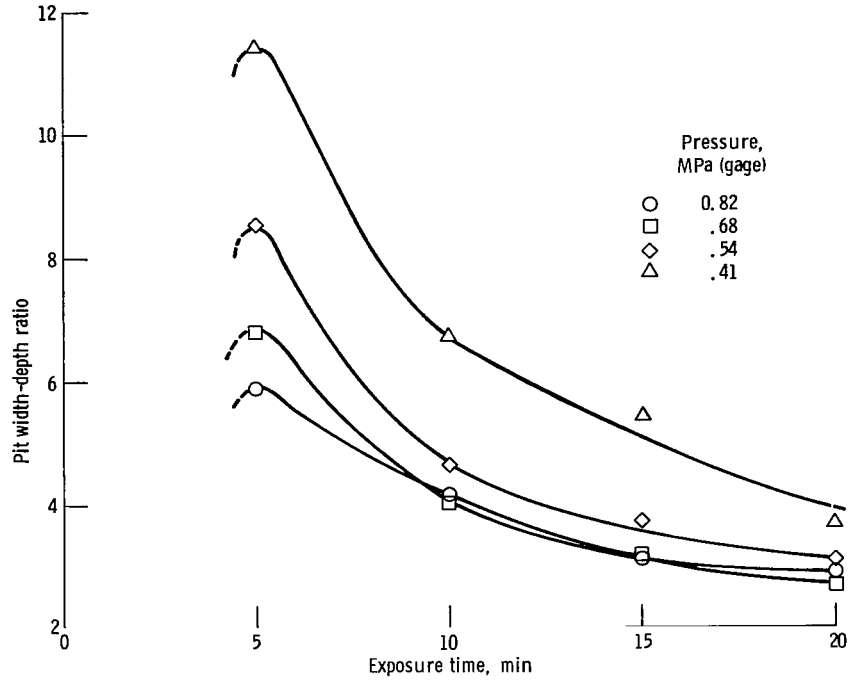

Figure 11. - Pit width-depth ratio as a function of exposure time for aluminum alloy exposed to jet of glass beads at different pressures.

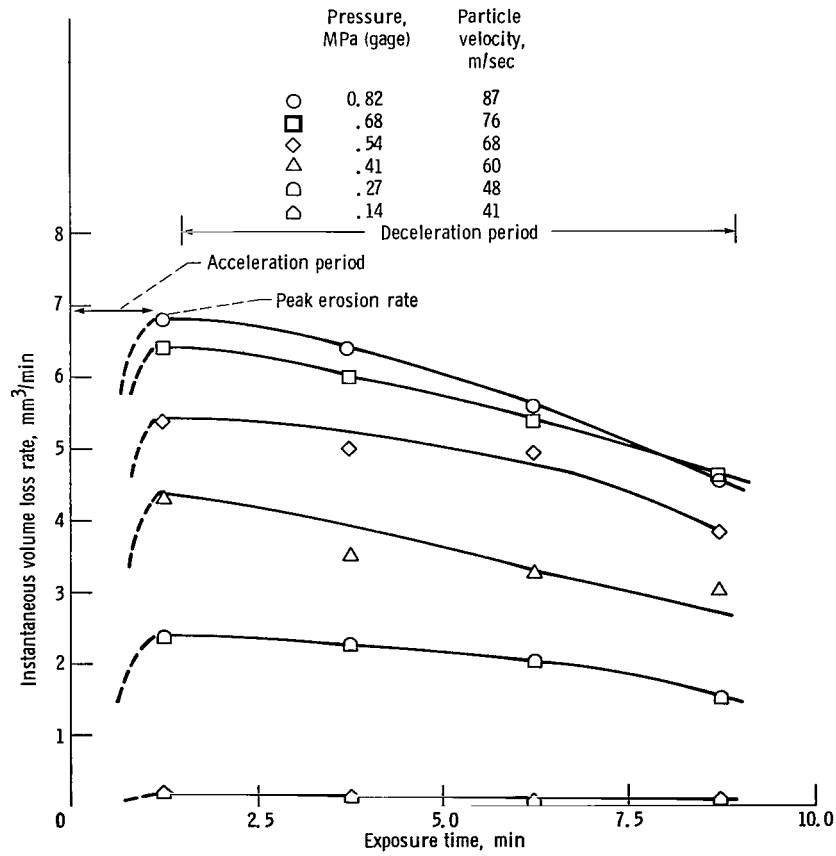

Figure 12. - Instantaneous volume loss rate as a function of exposure time for aluminum alloy exposed to jet of crushed glass at different pressures.

sizes of angular particles usually resulted in types I to III curves (fig. 2). These observations are discussed further in the next section.

Pit depth rate, pit width rate, and the width-depth ratio are presented as a function of exposure time in figures 13 to 15. All of the curves in figure 12 show an acceleration period, a peak erosion rate, and a deceleration period. Pit-depth-rate-versus-time curves (fig. 13) are similar to erosion-rate-versus-time curves (fig. 12). Pit-width-rate-versus-time and width-depth-ratio-versus-time curves (figs. 14 and 15) decelerate faster than did erosion-rate-versus-time curves. Hence, it can be assumed that pit depth rate predicts erosion rate to a larger extent than do pit width rate and the width-depth ratio. The latter, however, seems to influence the overall fluid-solid interaction process inside the pit once erosion is at an advanced stage.

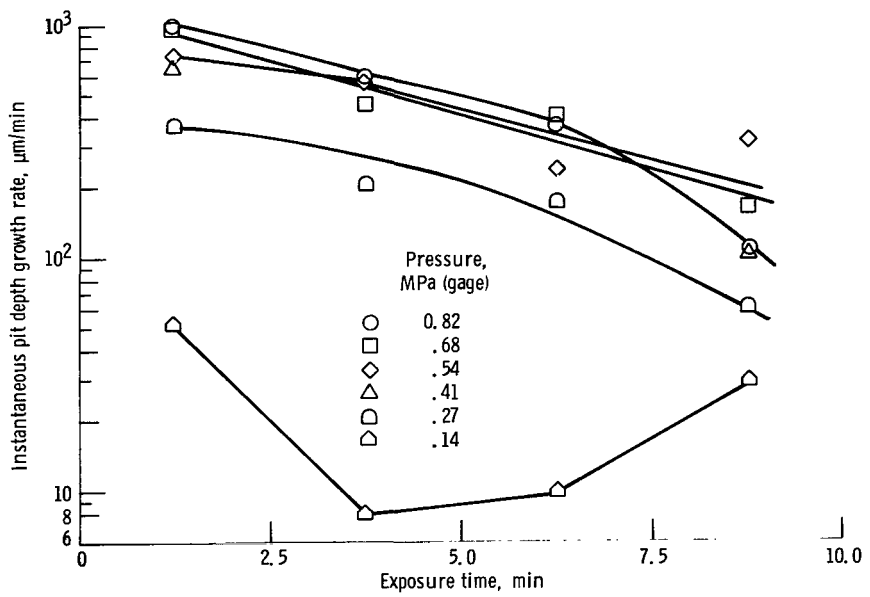

Figure 13. - Instantaneous pit depth growth rate as a function of exposure time for aluminum alloy exposed to jet of crushed glass at different pressures.

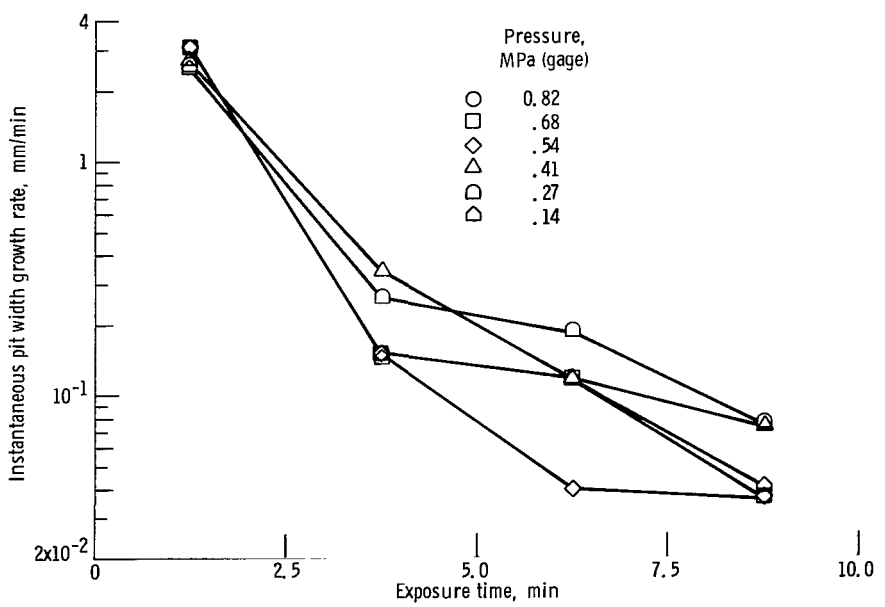

Figure 14. - Instantaneous pit width growth rate as a function of exposure time for aluminum alloy exposed to jet of crushed glass at different pressures.

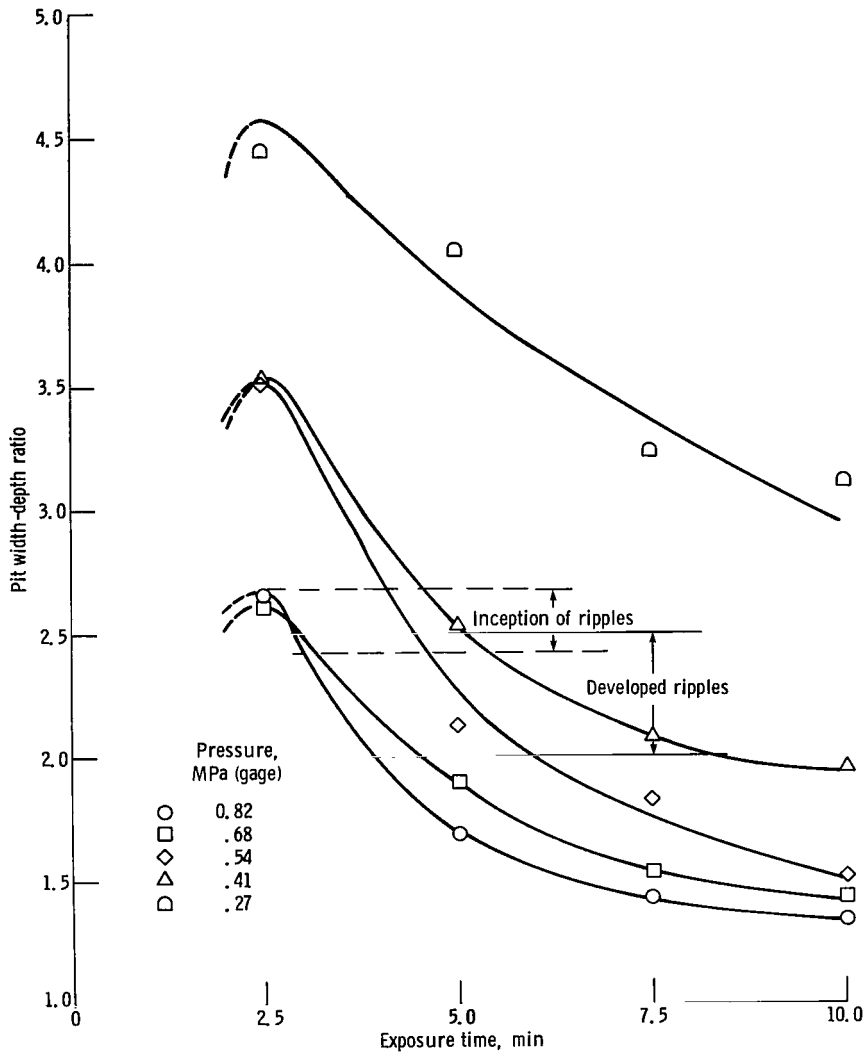

Figure 15. - Pit width-depth ratio as a function of exposure time for aluminum alloy exposed to jet of crushed glass at different pressures.

At long exposure times the depth of the pit may become sufficient to affect the erosion rate. A similar possibility is mentioned in reference 19. This results from two factors: an increase in the distance between the specimen and the jet nozzle, and a decrease in the velocity of the jet. References 25 and 27 found that both factors reduced the erosion rate.

Once the pit is very deep, the momentum of the jet has to almost reverse to push the particles out of the pit. Because of the confined nature of the pit, the jet may be cushioned or shielded by a layer of particles at the bottom of the pit. This can reduce the erosion rate in some situations.

Data Analysis from Different Types of Experiment Devices Reported in the Literature

To achieve an understanding of the general nature of the different types of erosion-rate-versus-time curves with reference (1) to particle shape and size and (2) to impact velocity, erosion data reported earlier (refs. 5 to 16, 18, and 20) were analyzed systematically.

Instantaneous weight loss rate as a function of abrasive charge, exposure time, or number of impacts for different materials tested at various experimental conditions

are presented in figures 16 to 25. The horizontal lines represent a least-squares fit of the data points on the linear portion of the curves. Normal impact experimental details (impact velocity, particle size, and particle flow rate) for each test as well as a discussion of weight loss-versus-time details are presented in table III.

Most of the curves in figures 16 to 24 conform to the type I and II curves (figs. 2(a) and (b)) when a smooth curve is drawn through the experimental points. Figure 25 conforms to a type III curve (figs. 2(c) and 5). (Some curves in figure 18 (steel) and figure 23 (151 m/sec) occasionally conform to the curves in figure 12, which have acceleration, peak erosion, and deceleration periods only.) This curve is schematically represented in figure 26 and is referred to as a type IV curve in this report. In this case the attainment of a steady-state period is doubtful except by approximation with a least-squares fit approach. As discussed earlier, type IV curves were observed in the present investigation (fig. 12) and are very rare.

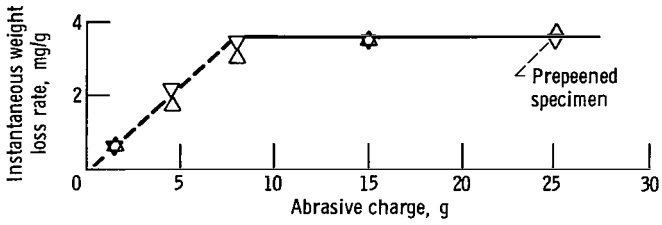

Figure 16. - Instantaneous weight loss rate as a function of abrasive charge for SAE 1020 steel exposed to jet of SiC particles at impact velocity of 76 m/sec and impingement angle of 90°. (Data from refs. 5 and 6.)

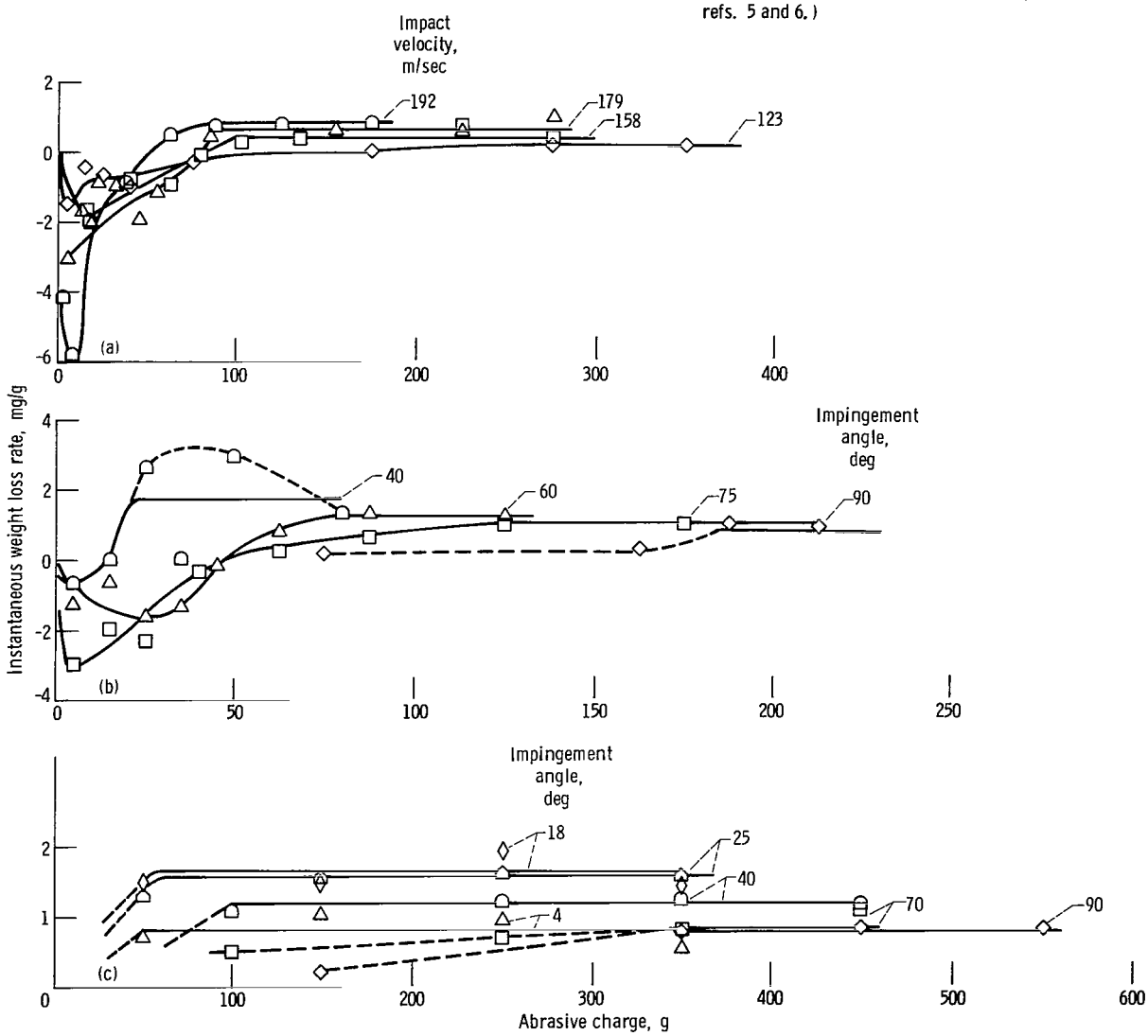

(a) Effect of impact velocity on deposition or embedment; impingement angle, 90°.
(b) Effect of impingement angle on deposition or embedment.
(c) Effect of impingement angle on erosion rate.

Figure 17. - Effect of impact velocity and impingement angle on deposition or embedment and on erosion rate for aluminum exposed to 210-μm-diameter Al_2O_3 particles. (Data from ref. 9.)

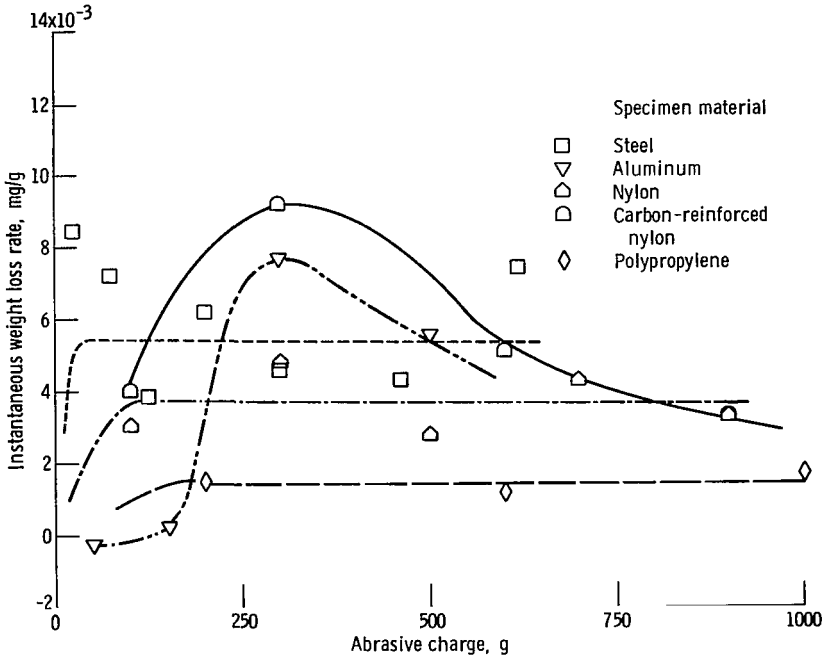

Figure 18. - Instantaneous weight loss rate as a function of abrasive charge for various materials exposed to normal incidence jet of quartz particles at impact velocity of 106 m/sec. (Data from ref. 13.)

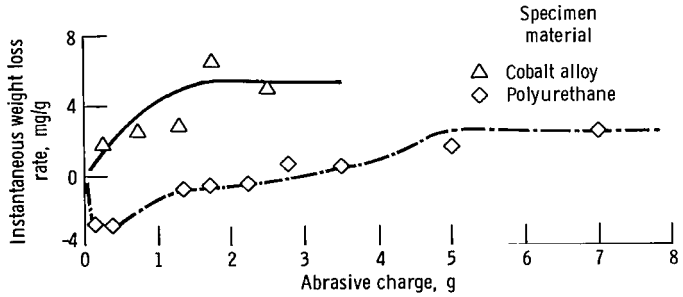

Figure 19. - Instantaneous weight loss rate as a function of abrasive charge for cobalt alloy and polyurethane exposed to jet of quartz particles at impact velocity of 128 m/sec and impact angle of 90°. (Data from ref. 14.)

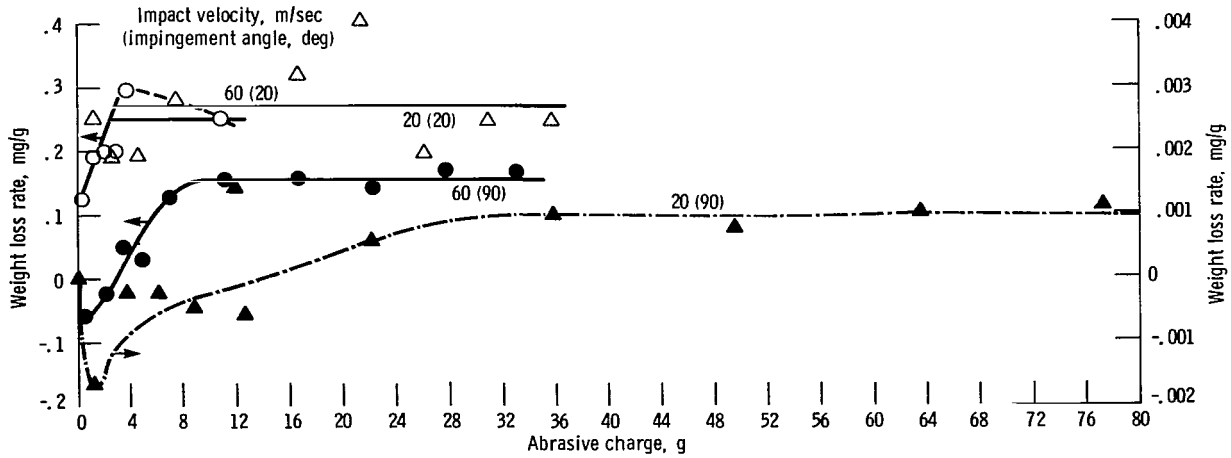

Figure 20. - Instantaneous weight loss rate as a function of abrasive charge. (Data from ref. 10).

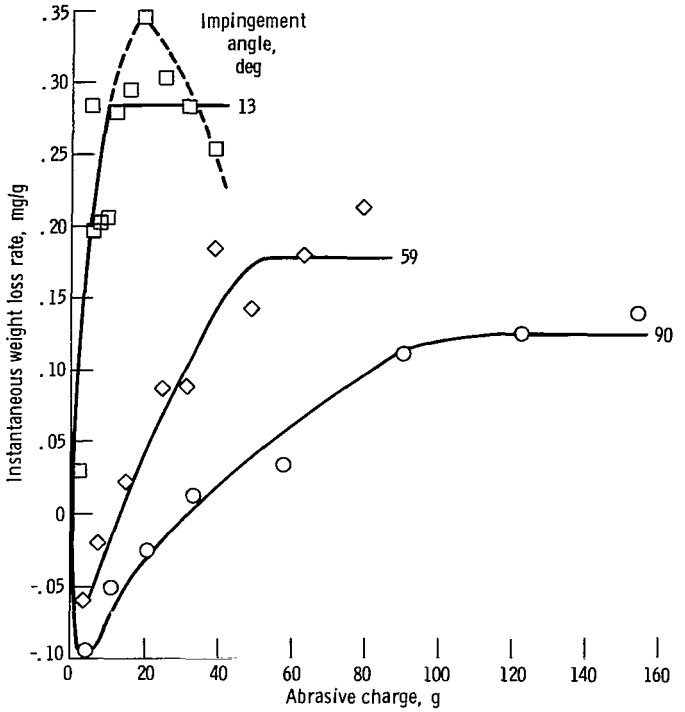

Figure 21. - Instantaneous weight loss rate as a function of abrasive charge for nickel exposed to jet of 149-μm-diameter Al_2O_3 particles at impact velocity of 53.8 m/sec. (Data from ref. 12.)

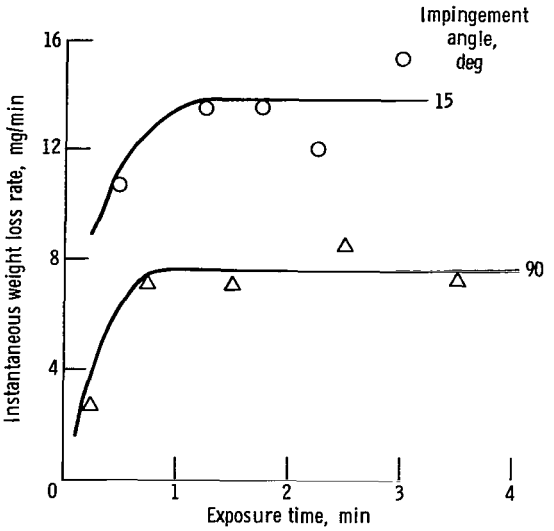

Figure 22. - Instantaneous weight loss rate as a function of exposure time for copper exposed to jet of 30-μm-diameter Al_2O_3 particles at impact velocity of 300 m/sec. (Data from ref. 11.)

The type of device including stationary or rotating specimen, the charge of erodent particles, jet impingement, or uniform flow did not seem to have much influence on the type of volume-loss-rate-versus-time curves (table III). However, the impact velocity, the impingement angle, and the shape and size of the particles probably influenced the shape of the curves to a considerable extent.

The effect of particle shape and size and impact velocity on erosion rate has been thoroughly discussed in references 1 to 3. The discrepancies of the exponential relationship between erosion rate and impact velocity have been highlighted in references 10, 15, and 16. The effect of particle shape and size and impact velocity on erosion-rate-versus-time curves and the trends of different periods from the overall data analysis are discussed in the following sections.

Particle Shape and Size

Angular particles caused maximum deposition at normal incidence angle; deposition, however, increased with decreasing velocity (fig. 17) and decreasing particle size (ref. 7) with slight exceptions. Spherical particles generally did not cause deposition or embedment. Hence, it may be surmised that with angular particles at normal incidence there is every possibility that erosion-rate-versus-time curves will conform to the type II curve (fig. 2(b)). When embedment took place, the steady-state erosion rate did not vary much in some situations (e.g., figs. 17 and 18). However, Tilly (ref. 28) states that as particle size increases particle fracture increases and results in more cutting type of erosion and embedment. In the experiments conducted by the present authors, the use of angular particles resulted in a special type of curve (type IV, fig. 12), which had been overlooked by other investigators. Spherical particles, however, resulted in type I and III curves (figs. 5 and 8). It may be recalled that the type III curve is not frequently observed and may be associated with pit geometry and cutting wear phenomena.

Impact Velocity

As impact velocity decreased, the scatter generally decreased and the erosion-rate-versus-time curve stabilized (ref. 7 and figs. 17 and 23). Higher impact velocities caused scatter and in some cases resulted in type IV erosion-rate-versus-time curves (fig. 26). As impact velocity decreased, deposition increased to initiate erosion (refs. 9 and 10). Hence the incubation and acceleration periods were long (fig. 17). The increase of both these periods is also evident from the results of the present authors (figs. 8 and 12) as velocity decreased (pressure decreased) for glass beads as well as crushed glass.

Stage of Erosion

Because four types of volume-loss-rate-versus-time curves (types I to IV, figs. 2 and 26) were observed under

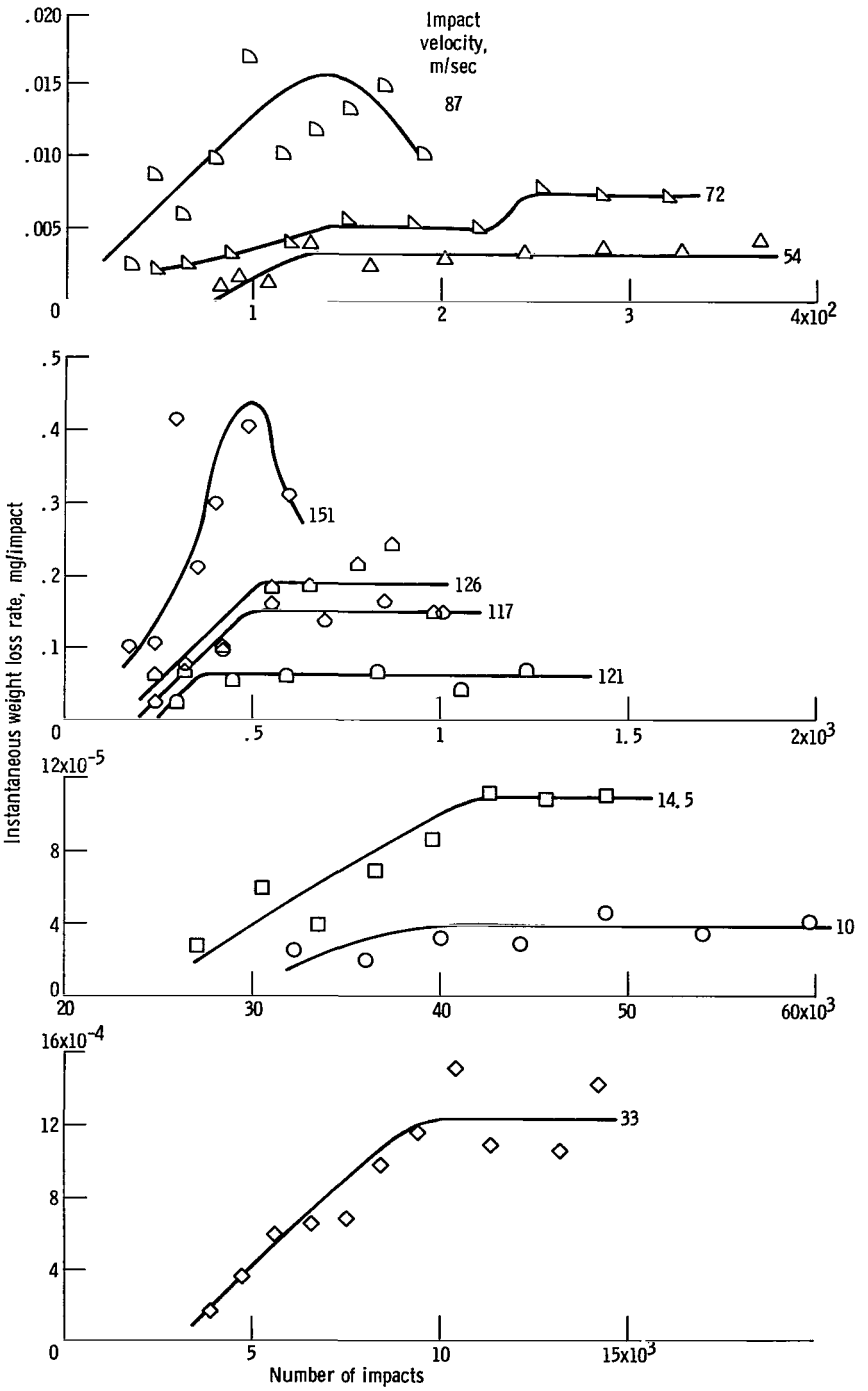

Figure 23. - Instantaneous weight loss rate as a function of number of impacts for pure aluminum surface exposed to jet of 70-μm-diameter glass spheres at different impact velocities. (Data from ref. 15.)

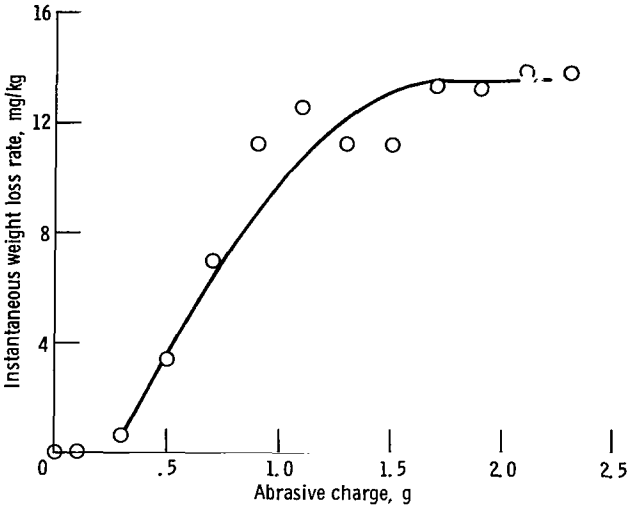

Figure 24. - Instantaneous weight loss rate as a function of abrasive charge for aluminum 6061-T6 exposed to jet of 495- to 600-μm-diameter glass beads at impact velocity of 64 m/sec and impingement angle of 90°. (Data from ref. 16.)

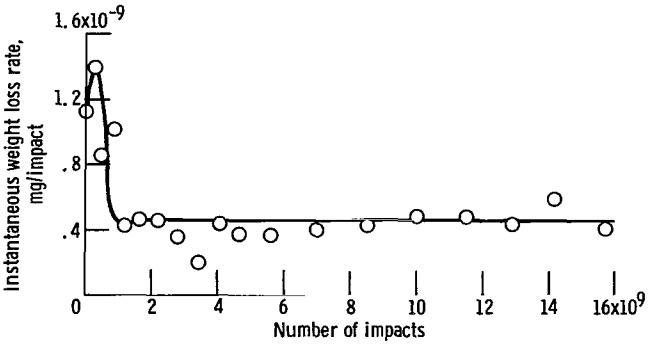

Figure 25. - Instantaneous weight loss rate as a function of number of impacts for copper exposed to jet of 50-μm-diameter glass spheres at impact velocity of 25 m/sec and impingement angle of 90°. (Data from ref. 18.)

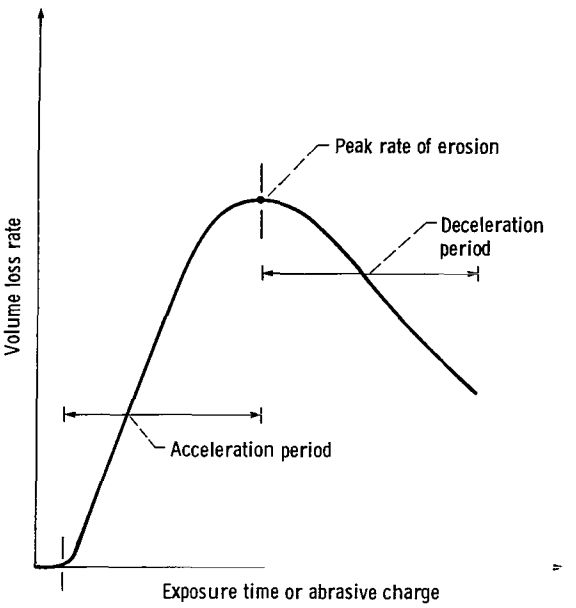

Figure 26. - Characteristic typical volume-loss-rate-versus-time curve (type IV).

vastly different experimental conditions, it is essential to consider a steady-state region or a peak erosion rate in characterizating and comparing experimental results for a wide spectrum of ductile materials. Large variations in the magnitude of erosion in the laboratory as well as in field situations suggest that test results should be compared only on the basis of corresponding stages and periods of the volume-loss-rate-versus-time curves. We believe that, if this is not done, scaling and modeling of erosion may not be precise and may result in errors.

Testing of various materials with a criterion of a fixed time interval is not the correct procedure for characterization and modeling efforts. To arrive at a steady-state period, the material specimen should be tested at equal time intervals to obtain an approximately constant volume loss. On the other hand, if there is considerable deviation of volume loss rate when a material is tested at fixed time intervals, the entire history of the erosion-versus-time curves should be obtained. Figures 5 and 25 of this report and figure 5 of reference 19 show that a spike in erosion rate is 150 to 300 percent higher than the steady-state erosion rate. Hence, the use of corresponding periods or stages of erosion in correlating and characterizing different materials is justified.

Estimation of Erosion Volume

Erosion pitting at any time represents the total erosion volume. The pits formed during glass-bead and crushed-glass impingement show two distinct shapes, as indicated in reference 29. It is therefore difficult to precisely calculate the volume of the eroded pit from spherical geometry. The erosion volume as a function of depth, width, and width-depth ratio of the pit for 6061-T6511 aluminum alloy specimens exposed to both forms of glass at different pressures and exposure times are presented in figures 27 to 29. The correlation coefficients and equations of the lines are presented in the figures. The slopes of the lines are approximately the same irrespective of the angular nature of the particles used.

Figures 27 to 29 indicate scatter despite the correct estimation of erosion volume. The correlation coefficients are more than 0.99 in all cases. It is further observed that the influence of exposure time and pressure (or velocity) conditions is negligible in this estimation irrespective of the type of erodent particles used. This result is interesting in the sense that impact by spherical microglass beads induced a pit shape similar to an

TABLE III. - DETAILS OF DIFFERENT TYPES OF EXPERIMENTAL EROSION DEVICES AND VOLUME-LOSS-RATE-VERSUS-TIME CURVES AT NORMAL INCIDENCE

Investigator(s)	Material	Abrasive (size)	Velocity, m/sec	Abrasive flow rate or exposure	Details of weight-loss-versus-time curve
Finnie (refs. 5 and 6)	SAE 1020 steel	SiC (60 mesh, 250 μm)	76	---	Curves exhibit cold working surface (slight incubation period at 90°), followed by weight loss proportional to the abrasive charge.
Neilson and Gilchrist (ref. 9)	Aluminum	Al_2O_3 (210 μm)	123 129 158 179 192	---	Linear portion of erosion-versus-abrasive-charge characteristics was obtained after deposition was stopped.
Tilly (ref. 13)	Chromium steel, aluminum, nylon, polypropylene, and carbon-reinforced nylon	Quartz (60 to 125 μm)	106	---	Experiments were probably influenced by the nonlinearity of the erosion rate for chromium steel. Significant incubation periods were exhibited for aluminum in both glancing and normal impacts.
Tilly and Sage (ref. 14)	Cobalt alloy and polyurethane	Quartz (125 to 150 μm)	128	---	Curves exhibit types of incubation behavior and a relatively small nonlinearity for metals but pronounced deposition followed by steady-state erosion for resilient plastics.
Ives and Ruff (ref. 10)	OFHC copper	Al_2O_3 (50 μm)	20,60	---	Specimen mass first increased and then decreased during a brief induction period.
Kosel, Scattergood, and Turner (ref. 12)	Nickel	Al_2O_3 (149 μm)	53.8	---	A constant rate of weight loss was achieved only after an initial transient period. Specimens eroded at normal incidence showed weight gains.
Carter, Nobes, and Arshak (ref. 11)	Copper	Al_2O_3 (30 μm) (irregularly shaped particles, mean diameter)	300	4 min	Curves exhibit a short induction period, followed by a steady-state period.
Rickerby and Macmillan (ref. 15)	Aluminum	WC - 6-percent Co spheres 1.58-mm diam)	10 14.5 33 54 72 87 101 117 126 151	---	Below a threshold number of impacts material removal was negligible. Erosion increased during succeeding incubation period[a] with increasing number of impacts, followed by a linear erosion period.
Hutchings (ref. 16)	Aluminum alloy 6061-T6	Glass beads (495 to 600 μm)	64	---	After an initial incubation period, sometimes characterized by a slight gain in specimen weight, the mass loss tended toward a linear dependence on the glass-bead particle mass.
Brown, Jun, and Edington (ref. 17)	Copper single crystal Iron	Glass spheres (70 μm)	122	7.2 g/min	Curves exhibit an incubation period,[a] followed by a steady-state period.
Follansbee, Sinclair, and Williams (ref. 18)	Copper (90°)	Glass spheres (50 μm)	25	---	No weight was gained. A linear rate of mass loss was obtained after an initial transient period.

[a]This period is called an incubation period by the authors; however, it is an acceleration period.

inverted probability distribution or a segment of a sphere. Crushed-glass particle impingement resulted in a paraboloid of revolution (ref. 29). All of the above correlations were found to be as accurate as the correlations between erosion volume and approximate pit volume. The equations presented in figures 27 to 29 estimate the erosion volume with respect to time by using only the depth, width, or width-depth ratio of a pit. This in turn intuitively provides a clue as to the universal nature of the theory of erosion irrespective of parameters involved or wear phenomena observed (deformation or cutting). The universal nature of erosion will be addressed in a subsequent paper.

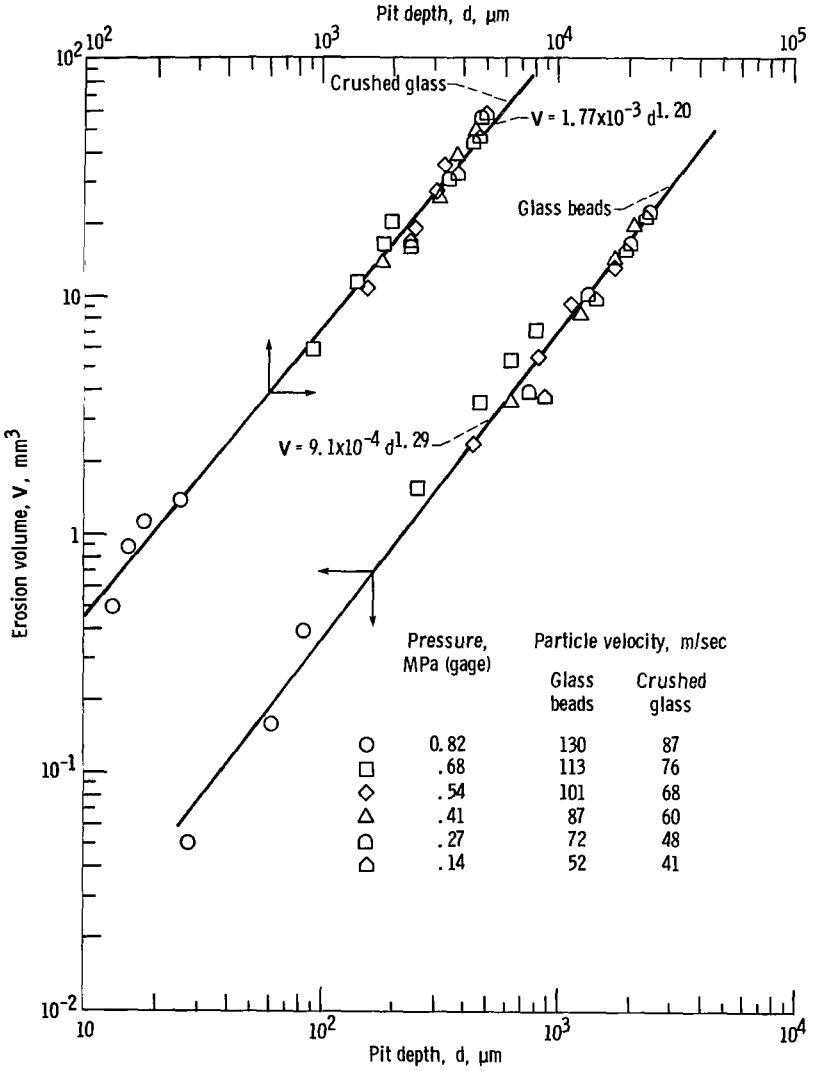

Figure 27. - Erosion volume as a function of pit depth.

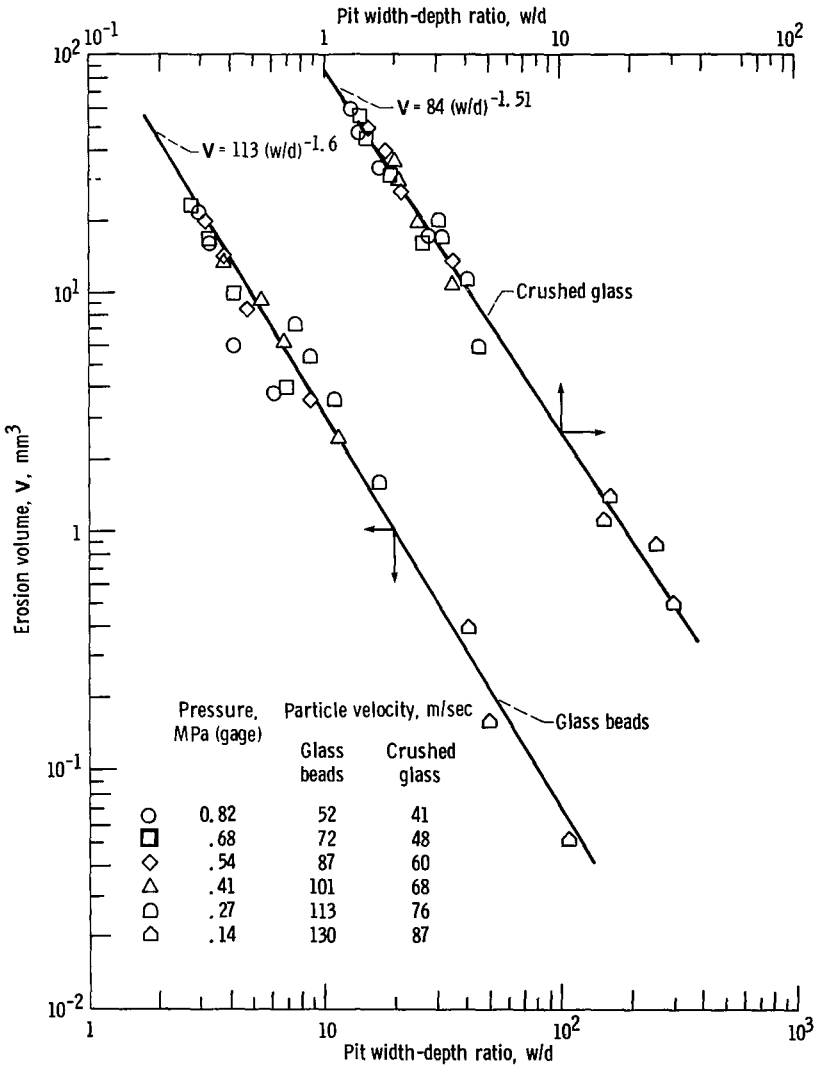

Figure 28. - Erosion volume as a function of width-depth ratio of the pit.

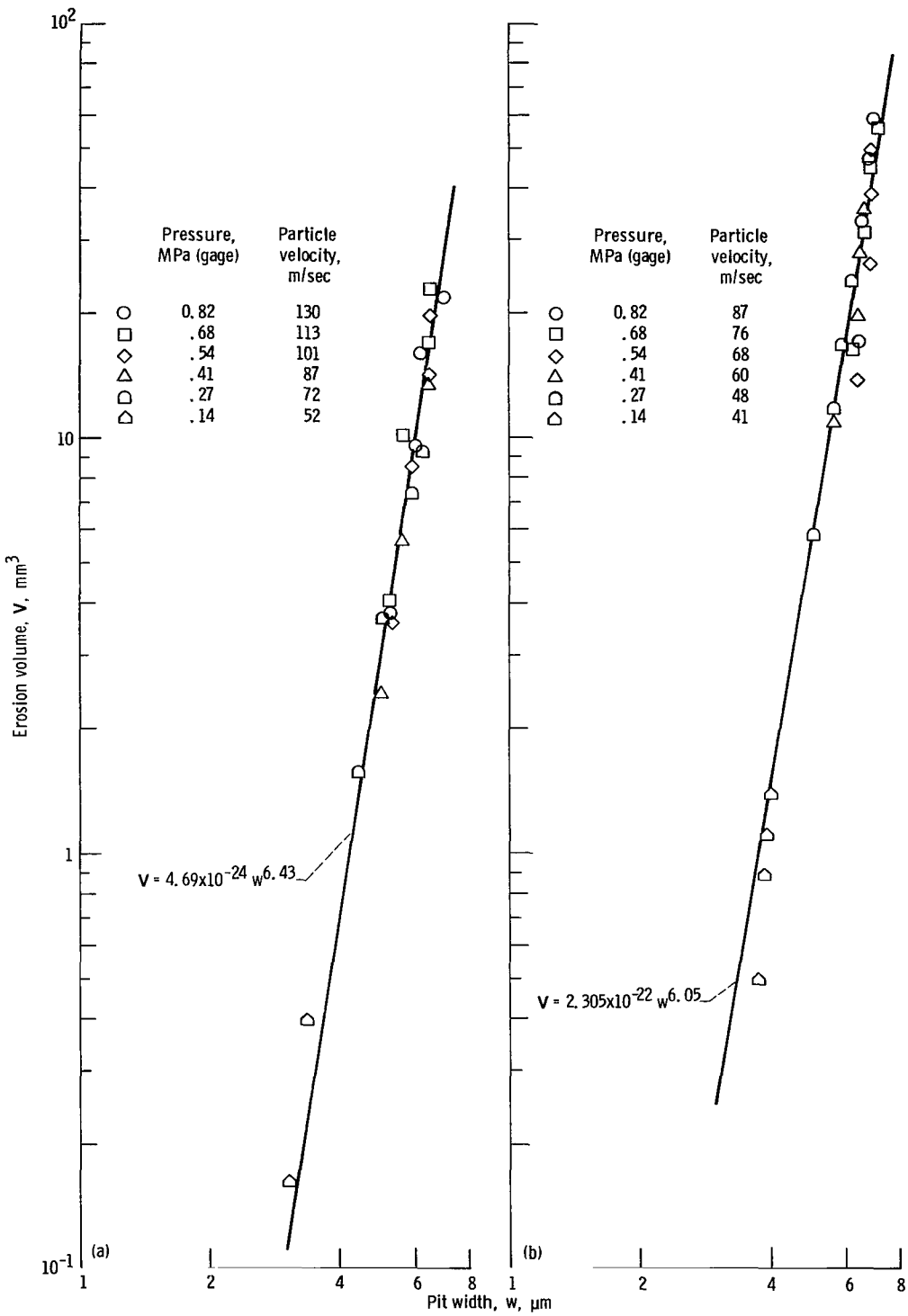

(a) Erodent, glass beads.
(b) Erodent, crushed glass.

Figure 29. - Erosion volume as a function of pit width.

Summary of Results

Volume-loss-versus-time curves obtained on 6061-T6511 aluminum alloy during normal jet impingement of glass beads and crushed-glass particles were analyzed. The effect of exposure time on erosion and hence the types of volume-loss-rate-versus-time curves were studied with respect to eroded pit morphology.

A large amount of experimental data in the literature was analyzed to investigate more thoroughly the effects of (1) the abrasive particle size and shape and (2) the impact velocity on erosion-rate-versus-time curves.

Studies with jets of glass beads and crushed-glass particles resulted in three different types of volume-loss-rate-versus-time curves: (1) curves with incubation, acceleration, and steady-state periods (type I); (2) curves with incubation, acceleration, deceleration, and steady-state periods (type III); and (3) curves with incubation, acceleration, peak rate, and deceleration periods (type IV). Type IV curves are rare and have not been reported by any other investigators.

The pit-width-versus-time or pit-depth-versus-time curves were similar to the cumulative erosion-versus-time curves for glass bead impingement. The pit-depth-rate-versus-time curves were similar to the volume-loss-rate-versus-time curves for crushed-glass impingement. In both cases the pit morphology (width, depth, and width-depth ratio) appeared to strongly control the volume-loss-rate-versus-time curves.

Analysis of a large amount of data from the literature indicated that under different experimental conditions three types of volume-loss-rate-versus-time curves emerge. Two types (types I and III) were observed in the present investigation, and the third type involves incubation (and deposition), acceleration, and steady-state periods (type II). With angular particles impinging at a normal angle of incidence, volume-loss-rate-versus-time curves conformed to the type II curve.

However, in a few cases actual points represented curves similar to a type IV curve. The incubation and acceleration periods increased with decreasing impact velocity.

Analysis of the present experimental results and data from the literature provided a strong understanding that the corresponding stages or periods of erosion must be considered in correlating and characterizing the erosion resistance of different materials.

Lewis Research Center
National Aeronautics and Space Administration
Cleveland, Ohio, February 18, 1983

References

1. Erosion Control in Energy Systems. NMAB-334, National Materials Advisory Board, Washington, D.C., 1977.
2. Adler, W. F.: Assessment of the State of Knowledge Pertaining to Solid Particle Erosion. Rept. ETI CR 79-680, U.S. Army Research Office, 1979.
3. Tilly, G. P.: Erosion by Impact of Solid Particles. Treatise on Materials Science and Technology, vol. 13, D. Scott, ed., Academic Press, New York, 1979, pp. 287-319.
4. Schmitt, G. F., Jr.: Liquid and Solid Particle Impact Erosion. Wear Control Handbook, M. P. Peterson and W. O. Winer, eds., American Society of Mechanical Engineers, New York, 1980, pp. 231-282.
5. Finnie, I.: The Mechanism of Erosion of Ductile Metals. Proc. 3rd U.S. National Congress of Applied Mechanics, American Society of Mechanical Engineers, New York, 1958, pp. 527-532.
6. Finnie, I.: Erosion of Surfaces by Solid Particles. Wear, vol. 3, 1960, pp. 87-103.
7. Duffin, H. C.: A Laboratory Scale Study of Erosion and Deposition due to Gas Borne Solids. NGTE-M-341, National Gas Turbine Establishment, Aug. 1960.
8. Finnie, I.; Wolak, J.; and Kabil, Y.: Erosion of Metals by Solid Particles. J. Mater., vol. 2, Sept. 1967, pp. 682-700.
9. Neilson, J. H.; and Gilchrist, A.: Erosion by a Stream of Solid Particles. Wear, vol. 11, 1968, pp. 111-121.
10. Ives, L. K.; and Ruff, A. W.: Electron Microscope Study of Erosion Damage in Copper. Erosion: Prevention and Useful Applications. W. F. Adler, ed., Am. Soc. Test. Mater. Spec. Tech. Publ. (664), 1977, pp. 5-35.
11. Carter, G.; Nobes, M. J.; and Arshak, K. I.: The Mechanism of Ripple Generation on Sandblasted Ductile Solids. Wear, vol. 65, 1980, pp. 151-174.
12. Kosel, T. H.; Scattergood, R. O.; and Turner, A. P. L.: An Electron Microscope Study of Erosive Wear. Wear of Materials 1979, K. C. Ludema, W. A. Glaeser, and S. K. Rhee, eds., American Society of Mechanical Engineers, New York, pp. 192-204.
13. Tilly, G. P.: Erosion Caused by Airborne Particles. Wear, vol. 14, 1969, pp. 63-79.
14. Tilly, G. P.; and Sage, W.: A Study of the Behavior of Particles and Materials in Erosion Processes. ASME Paper 69-WA/Met-6, 1969.
15. Rickerby, D. G.; and Macmillan, N. H.: The Erosion of Aluminum by Solid Particle Impingement at Normal Incidence. Wear, vol. 60, no. 2, 1980, pp. 369-382.
16. Hutchings, I. M.: A Model for the Erosion of Metals by Spherical Particles at Normal Incidence. Wear, vol. 70, no. 3, 1981, pp. 269-281.
17. Brown, R.; Jun, E.-J.; and Edington, J. W.: Mechanisms of Solid Particle Erosive Wear for 90° Impact on Copper and Iron. Wear, vol. 74, no. 1, 1981, pp. 143-156.
18. Follansbee, P. S.; Sinclair, G. B.; and Williams, J. C.: Modeling of Low Velocity Particulate Erosion in Ductile Materials by Spherical Particles. Wear, vol. 74, no. 1, 1981, pp. 107-122.
19. Young, J. P.; and Ruff, A. W.: Particle Erosion Measurements on Metals. J. Eng. Mater. Technol., vol. 99, no. 2, Apr. 1977, pp. 121-125.
20. Söderberg, S.; et al.: Erosion Classification of Materials Using a Centrifugal Erosion Tester. Tribol. Int., vol. 14, no. 6, Dec. 1981, pp. 333-343.

21. Rao, P. Veerabhadra; Young, S. G.; and Buckley, D. H.: Morphology of Ductile Metals Eroded by Spherical Particles Impinging at Normal Incidence. Wear, vol. 85, no. 2, 1983, pp. 223-237.
22. Chao, C.; et al.: ASTM Round-Robin Test with Vibratory Cavitation and Liquid Impact Facilities of 6061-T6511 Aluminum Alloy, 316 Stainless Steel, and Commercially Pure Nickel. Report No. MMPP-344-3-T, University of Michigan, 1968.
23. Rao, P. Veerabhadra; Young, S. G.; and Buckley, D. H.: Solid Spherical Glass Particle Impingement Studies of Plastic Materials. NASA TP-2161, 1983.
24. Salik, J.; and Buckley, D. H.: Effect of Erodent Particle Shape and Various Heat Treatments on Erosion Resistance of Plain Carbon Steel. NASA TP-1755, 1981.
25. Ruff, A. W.; and Ives, L. K.: Measurement of Solid Particle Velocity in Erosive Wear. Wear, vol. 35, 1975, pp. 195-199.
26. Rao, P. Veerabhadra; Young, S. G.; and Buckley, D. H.: Morphology of an Aluminum Alloy Eroded by a Jet of Angular Particles Impinging at Normal Incidence. NASA TP-2139, 1983.
27. Wolak, J.; et al.: Parameters Affecting the Velocity of Particles in an Abrasive Jet. J. Eng. Mater. Technol., vol. 99, no. 2, Apr. 1977, pp. 147-152.
28. Tilly, G. P.: A Two-Stage Mechanism of Ductile Erosion. Wear, vol. 23, 1973, pp. 87-96.
29. Rao, P. Veerabhadra; Young, S. G.; and Buckley, D. H.: A Study of the Nature of Solid Particle Impact and Shape on the Erosion Morphology of Ductile Metals. NASA TM-82933, 1982.

1. Report No.	2. Government Accession No.	3. Recipient's Catalog No.
NASA TP-2169		

4. Title and Subtitle	5. Report Date
TIME DEPENDENCE OF SOLID-PARTICLE IMPINGEMENT EROSION OF AN ALUMINUM ALLOY	August 1983
	6. Performing Organization Code 506-53-1B
7. Author(s)	8. Performing Organization Report No.
P. Veerabhadra Rao and Donald H. Buckley	E-1381
	10. Work Unit No.
9. Performing Organization Name and Address	
National Aeronautics and Space Administration Lewis Research Center Cleveland, Ohio 44135	11. Contract or Grant No.
	13. Type of Report and Period Covered
12. Sponsoring Agency Name and Address	Technical Paper
National Aeronautics and Space Administration Washington, D. C. 20546	14. Sponsoring Agency Code

15. Supplementary Notes P. Veerabhadra Rao, National Research Council - NASA Research Associate; Donald H. Buckley, Lewis Research Center. Presented in part at the 6th International Conference on Erosion by Liquid and Solid Impact, Cambridge, England, Sept. 4-8, 1983, as paper entitled Time Effect of Erosion by Solid Particle Impingement on Ductile Materials (NASA TM-83369).

16. Abstract

Erosion studies were conducted on 6061-T6511 aluminum alloy by using jet impingement of glass beads and crushed-glass particles to investigate the influence of exposure time on volume loss rate at different pressures. The results indicate a direct relationship between erosion-versus-time curves and pit-morphology (width, depth, and width-depth ratio)-versus-time curves for both glass forms. Extensive erosion data from the literature were analyzed to find the variations of erosion-rate-versus-time curves with respect to the type of device, the size and shape of erodent particles, the abrasive charge, the impact velocity, etc. Analysis of the present experimental data, obtained with two forms of glass, resulted in three types of erosion-rate-versus-time curves: (1) curves with incubation, acceleration, and steady-state periods (type I); (2) curves with incubation, acceleration, deceleration, and steady-state periods (type III); and (3) curves with incubation, acceleration, peak rate, and deceleration periods (type IV). The type IV curve is a less frequently seen curve and had not been reported in the literature. Analysis of extensive literature data generally indicated three types of erosion-rate-versus-time curves. Two types (types I and III) were observed in the present study; the third type involves incubation (and deposition), acceleration, and steady-state periods (type II). Examination of the extensive literature data indicated that it is absolutely necessary to consider the corresponding stages or periods of erosion in correlating and characterizing erosion resistance of a wide spectrum of ductile materials.

17. Key Words (Suggested by Author(s))		18. Distribution Statement
Solid impingement	Time dependence	Unclassified - unlimited
Ductile metals	Aluminum alloy	STAR Category 26
Erosion	Particle impact	
Erosion rate		

19. Security Classif. (of this report)	20. Security Classif. (of this page)	21. No. of Pages	22. Price*
Unclassified	Unclassified	23	A02

* For sale by the National Technical Information Service, Springfield, Virginia 22161

NASA-Langley, 1983

National Aeronautics and Space Administration

Washington, D.C.
20546

Official Business
Penalty for Private Use, $300

THIRD-CLASS BULK RATE

Postage and Fees Paid
National Aeronautics and
Space Administration
NASA-451

U.S.MAIL

5 1 1U,C, 830810 S00903DS
DEPT OF THE AIR FORCE
AF WEAPONS LABORATORY
ATTN: TECHNICAL LIBRARY (SUL)
KIRTLAND AFB NM 87117

S

NASA

POSTMASTER: If Undeliverable (Section 158 Postal Manual) Do Not Return